Lateral Stability of Rigid Poles Subjected to a Ground-Line Thrust

ROBERT L. KONDNER, Civil Engineering Department, Technological Institute, Northwestern University; and
GORDON E. GREEN, Shannon and Wilson, Consulting Engineers, Seattle

Functional relationships are developed for the load-deflection characteristics of rigid, vertical poles, embedded in sand, subjected to a horizontal ground-line thrust and ground-line couple-moment. The study is based on nondimensional techniques and the physical variables included in the theoretical analysis are the ground-line deflection, depth of embedment, geometry of the pole cross-section, ground-line thrust, couple-moment at the ground-line, time of loading, and soil parameters. The soil parameters used are the density, angle of internal friction, and flow viscosity of sand. Nondimensional techniques in conjunction with small-scale model studies are used to determine the interrelationship among these physical variables for a pole embedded in a dense, uniform, fine dune sand of constant properties and subjected to a horizontal ground-line thrust only. Prediction equations are given from which the load-deflection characteristics of a prototype pole might be determined. A failure criterion relating the ultimate ground-line thrust to the pole geometry and examples are given.

•POLES subjected to lateral loads are used extensively by utilities, railroads, highway departments, and outdoor advertising agencies. The lateral stability of a pole has, to date, defied any altogether satisfactory analysis although numerous authors have attempted to solve the problem both analytically and empirically. At present, design is usually based on past experience, empirical formulas, or inadequate theoretical analyses founded on unrealistic assumptions. To obtain a rigorous solution to the problem of a partially embedded pole, certain systems of equations must be solved. The solution must satisfy the equilibrium equation, compatibility equations, and boundary conditions. Any solution will depend on the form of the stress-strain-time relationships used for the soil, and herein lies the difficulty. In general there are no stress-strain-time relationships available for soils.

This investigation was aimed at describing the phenomena of pole-soil behavior by determining the relationships among the physical variables involved through a semi-empirical approach utilizing dimensional analysis and small-scale model experiments on sand. The methods of dimensional analysis which have proved successful in other fields with regard to model-prototype studies were used in an attempt to achieve a coherent rational order to the study. It has been shown by Kondner (1, 2, 3, 4) that the use of these methods in soil mechanics is advantageous. Model tests have great flexibility with regard to the number of variables and conditions that can be studied in a given time. They should however be correlated with field experience.

A pole or short pile is essentially a partially embedded rigid member whose lateral deflections, under load, are primarily due to rigid body motions. It is assumed that flexural failure of the pole does not occur and that failure of the soil may be assumed to have occurred when the angle of inclination θ of the pole with the vertical becomes excessive.

The research reported in this paper involved a study of the following factors:

1. The development of a theoretical, nondimensional, functional form of the parameters involved in the load-deflection-time relationship for a laterally loaded single pole partially embedded in sand. This includes both horizontal ground-line thrust and ground-line couple-moment.
2. The design and calibration of a model to perform tests on poles embedded in sand of constant properties which are subjected to a horizontal ground-line thrust only.
3. Tests on the model to determine the load-deflection-time relationship involved, considering (a) reproducibility of test results, (b) influence of creep phenomena to determine a suitable loading rate, (c) effect of varying the loading rate on the load-deflection relationship, and (d) effect of varying the diameter and depth of embedment of the pole on the load-deflection-time relationship.
4. An analysis of the model test results to develop an empirical equation relating the physical variables involved.
5. Construction of nomographs to predict (a) failure loads and (b) load-deflection relationships for a pole embedded in dense dry sand having constant properties and subjected to a horizontal ground-line thrust.

Although the general pole problem containing thrusts and couple-moments has been functionally formulated for both cohesive and cohesionless soils, the primary emphasis of the present paper deals with only one phase of the problem, ground-line thrusts and sand, and as such is the first of a series of papers on the general problem. Future papers will deal with couple-moments and superposition principles in sands and clays as well as ground-line thrusts in clays. In addition, the study presented herein deals only with a very dense, uniform sand having a constant dry density of 107 pcf. Preliminary tests indicate that the important soil parameter effecting the load-deflection response of poles partially embedded in sands is the relative density of the sand. Relative density effects will be studied in the near future.

EXISTING INFORMATION

Beginning in the early 1920's a relatively large number of papers have appeared that attempt to solve the laterally loaded single pole problem. According to Prakash (5), the majority of analytical solutions are based on one or more of the following assumptions:

1. The maximum resistance to deformation of the soil at any depth is equal to Rankine's passive earth pressure or the difference between Rankine's active and passive earth pressures at that depth.
2. To develop passive resistance there must be movement (however small) of the pole compressing the ground in front of it.
3. The intensity of passive resistance developed is proportional to the amount of lateral displacement.
4. The intensity of the passive resistance developed is proportional to the depth below the ground-line.

In addition, individual authors have made further assumptions, particularly with respect to the shape of the pressure distribution diagram. An excellent annotated bibliography by Chang (6) concerning laterally loaded piles contains a chronological summary of the literature up to 1958, which includes poles as a subsection. The more extensive work by Prakash (5) contains a fairly complete review confined to the behavior of partially embedded poles subjected to lateral loads. In view of the availability of these two papers, it is not proposed to submit an extensive review of previous authors' work. This review will confine itself to some of the more recent trends and their implications.

There is no clear agreement in the literature as to a definition of the problem. Most authors assume a vertical pole with a horizontal load applied above the ground-line whereas Prakash (5) has considered the additional effect of a vertical load and an initial inclination of the axis of the pole. Considering the difficulty of the pole-soil

interaction, it would seem rational to study the simplified cases first and build up to the more general pole system.

The rotation of a laterally loaded pole requires that large deformations occur near the ground surface, where the soil is least capable of offering resistance. Therefore, the soil near the ground surface will probably nearly always be in a "plastic" state when resisting a laterally loaded pole. At some depth below the ground surface the soil behavior becomes nearly elastic. Thus, according to Prakash (5) a combination of elastic and plastic soil behavior should be accounted for in an analysis of a laterally loaded pole. According to Terzaghi (7) the deformation characteristics of a stiff clay are more or less independent of depth. However, the strength characteristics of clay soils may increase or decrease with depth, depending on the geographical location and climate, so that no general rules may be formulated. In connection with clay, on account of progressive deflection under constant load (a creep effect), the deformation increases and the soil modulus function varies with time—both approaching ultimate values. Ideally, these ultimate values should be used in the analysis. In a cohesionless sand the values of the deformation and the soil modulus are supposedly independent of time, but the soil modulus increases approximately in simple proportion to depth. According to Czerniak (8), the analysis is further complicated because the sand may fill the space left as the pole moves, thus preventing its returning to the vertical position upon removal of the overturning forces. An analytical solution of the laterally loaded pole is hence stymied by the unknown soil stress-strain-time relation which is herein called the soil modulus function. Present trends in analytical studies favor an increase in the soil modulus function in direct proportion to depth for sands:

$$k_x = k_h x \tag{1}$$

in which

k_x = soil modulus function at depth x,

k_h = constant of horizontal subgrade reaction function, and

x = depth below ground level.

For cohesive soils Palmer and Thompson (9) consider that:

$$k_x = k_h \frac{x^n}{L} \tag{2}$$

in which

L = depth of embedment and

k_h = constant

adequately describes the variation of soil modulus with depth and they indicate that the values for n must be determined by applying the method to check various field data.

Matlock and Reese (10) attempted to derive generalized solutions for laterally loaded piles, treating the rigid pole as a particular case. They considered the nonlinear force-deformation-depth characteristics of the soil by means of the repeated application of elastic theory. The soil modulus constants were adjusted for each successive trial until satisfactory compatibility was obtained between the predicted behavior of the soil and the load-deflection relationships required by the pole. In the final trial, in a series of iterative approximations, the final variation in soil modulus could assume any form with respect to distance along the pole. If it were required that the soil modulus values be adjusted independently at each depth considered, then, in practice, a solution for any particular pole problem required the use of a digital computer. The author gave nondimensional general solutions that could be computed for any desired form of variation of soil modulus with respect to depth. However, the two general forms of soil modulus function, the power form,

$$E_s = kx^n \tag{3}$$

and the polynomial form,

$$E_s = k_o + k_1 x \tag{4}$$

which the authors considered suitable are perhaps oversimplifications and may not be sufficiently sensitive to characterize the soil-pole interaction.

In an attempt to circumvent the soil modulus-depth-deflection-time relationship problem, it was believed that the behavior of the soil could be defined by parameters that could be more easily measured and controlled than the soil modulus. This, in conjunction with a semiempirical approach making use of small-scale model experiments, designed and constructed on the basis of the methods of dimensional analysis, seems to be a feasible method of attacking the problem.

THEORETICAL ANALYSIS

To describe a physical phenomena it is necessary to define it in terms of a finite number of physical quantities or parameters. Dimensional analysis offers an easy way to formulate such a description in functional form. The method of dimensional analysis as used to formulate relationships between physical quantities can be briefly summarized as follows. If there are m physical quantities containing n fundamental units, which can be related by an equation, then there are (m-n), and only (m-n), independent, nondimensional parameters (called π-terms) such that the π-terms are arguments of some indeterminate, homogeneous function $\varkappa$:

$$\varkappa\ (\pi_1, \pi_2, \pi_3, \ldots, \pi_{m-n}) = 0. \tag{5}$$

An important part of the dimensional analysis is the choice of the physical quantities involved. Once this is accomplished, a methodical process is used to obtain the π-terms contained in the functional formulation. The functional formulation is the extent to which dimensional analysis is useful. The explicit form of the functional relation must then be determined experimentally.

To keep the explicit form of the functional relation as simple as possible, only the more important variables should be considered. If the number of variables considered is too large, the practical usefulness of the results may be greatly impaired. In addition, the difficulties involved in the separation of the nondimensional parameters in the experimental determination of the explicit nature of the functional relation will be quite formidable. However, should important variables that may logically influence the phenomenon be omitted, the experimental phase may be simple, but the results may be incomplete or erroneous.

The analysis of a laterally loaded pole embedded in the ground is a static problem. The boundary forces have a predominating influence in the problem rather than the body forces and the latter will be neglected in the subsequent analyses. The general methods of dimensional analysis have been described elsewhere (11, 12) and are repeated here. The particular problems encountered in the soil mechanics field when applying this tool have been described by Kondner (1) and his techniques are freely drawn on in the analyses where considered desirable.

It is assumed that the material constants needed to describe the deformation characteristics of the sand are implicit in the dry density, angle of internal friction, and "viscosity" of the sand. The term "viscosity" refers to the time-dependent deformation characteristics that were observed in the experimental program. It has been previously noted that the relative density is thought to be an important soil parameter, but is by definition nondimensional and can be added to the functional relationship when convenient. For the present study the relative density was held constant and hence is not specifically included as a variable. A future test series will be conducted in which various relative densities will be studied.

The physical quantities considered in this study are given in Table 1. A force, length, and time system of fundamental units has been used. Because there are ten physical quantities and three fundamental units, there must be seven independent,

TABLE 1

PHYSICAL QUANTITIES CONSIDERED IN THE DIMENSIONAL ANALYSIS OF A RIGID POLE EMBEDDED IN SAND

Quantity	Symbol	Fundamental Unit
Deflection at ground-line	y	L
Depth of embedment	L	L
Cross-sectional area of pole	A	L^2
Perimeter of pole	C	L
Thrust at ground-line	F	F
Moment at ground-line	M	FL
Dry density of sand	γ	FL^{-3}
Angle of internal friction	ϕ	$F^\circ L^\circ T^\circ$
Viscosity of sand	η	$FL^{-2}T$
Time of loading	t	T

nondimensional π-terms. These π-terms can be methodically obtained by choosing three physical quantities that contain all three fundamental units and cannot be formed into a nondimensional parameter by themselves (for example, F, t, and L), and combining them with each of the remaining quantities one at a time. As an example, combining them with γ,

$$\pi = F^{\alpha} \cdot t^{\beta} \cdot L^{\rho} \cdot \gamma^{\lambda} = F^{\circ} L^{\circ} T^{\circ} \tag{6}$$

Substituting the fundamental units of each of the physical quantities involved into Eq. 6,

$$(F)^{\alpha} \cdot (T)^{\beta} \cdot (L)^{\rho} \cdot (FL^{-3})^{\lambda} = F^{\circ} L^{\circ} T^{\circ} \tag{7}$$

Equating exponents of the fundamental units,

$$\begin{aligned} \alpha + \lambda &= 0, \\ \beta &= 0, \text{ and} \\ \rho - 3\lambda &= 0 \end{aligned} \tag{8}$$

Solving Eq. 8 by letting $\alpha = 1$ gives

$$\alpha = 1 \ , \ \beta = 0 \ , \ \rho = -3 \ , \text{ and } \lambda = -1 \tag{9}$$

Thus, the π-term under consideration is

$$\pi = \frac{F}{\gamma L^3} \ . \tag{10}$$

By repeating this process for the other physical quantities involved, the following nondimensional parameters can be obtained:

$$\bar{\pi}_1 = \frac{y}{L}, \ \bar{\pi}_2 = \frac{A}{L^2}, \ \bar{\pi}_3 = \frac{C^2}{L}, \ \bar{\pi}_4 = \frac{M}{FL}, \qquad \bar{\pi}_5 = \frac{F}{\gamma L^3} \quad \bar{\pi}_6 = \phi \ , \text{ and } \bar{\pi}_7 = \frac{Ft}{L^2 \eta} \tag{11}$$

Because a requirement of the function $\varkappa$ is that it shall consist of independent, non-

dimensional parameters, there is nothing unique about these forms of the π-terms. It is therefore possible to transform the π-terms algebraically in any way desired so long as the final π-terms are nondimensional and independent. The final form is chosen so as to group desired physical quantities together in the most meaningful form; in particular with regard to the form of the experimental data. This implies that each term shall preferably contain one and only one physical quantity having a predominating effect on the function $\varkappa$.

By algebraically transforming Eq. 11 the following form of the π-terms was obtained:

$$\pi_1 = \frac{y}{L}, \quad \pi_2 = \frac{C}{L}, \quad \pi_3 = \frac{C^2}{A}, \quad \pi_4 = \frac{F}{\gamma AL}, \qquad (12)$$

$$\pi_5 = \frac{\gamma tc}{\eta}, \quad \pi_6 = \frac{M}{\gamma AL^2}, \quad \pi_7 = \phi$$

The π-terms of Eq. 12 may be substituted into Eq. 5 to obtain the functional relationship which can be rewritten

$$\frac{y}{L} = \varkappa\left[\frac{C}{L}, \frac{C^2}{A}, \frac{F}{\gamma AL}, \frac{\gamma tC}{\eta}, \frac{M}{\gamma AL^2}, \phi\right] \qquad (13)$$

In Eq. 13 and hereafter the symbol $\varkappa$ denotes "some function of," but not necessarily the same function for, each equation. This notation is used to avoid the use of numerous subscripts and superscripts as a means of differentiating between the equations.

The physical interpretation of the π-terms contained in Eq. 13 is as follows. The dependent variable is the term y/L which is called the deflection ratio. This term is the ratio of the horizontal surface deflection to the depth of embedment. Shape effects are given by C^2/A which is the characteristic shape factor of the pole. For a circular cross-section of any size, the shape factor is equal to 4π ($\pi = 3.1416$), and for a square shape the value is 16. The term C/L is a geometric factor pertaining to the distribution of the cross-section area of the pole and is called the slenderness ratio. The term $F/\gamma AL$ is the ratio of the applied force to the resisting force and is called the thrust strength ratio. The term $M/\gamma AL^2$ is the ratio of the applied moment to the resisting moment and is called the moment strength ratio. Creep effects are included in the term $\frac{\gamma tC}{\eta}$ which is considered to be the ratio of the time of loading to a characteristic relaxation time of the soil. The angle of internal friction (ϕ) is, by definition, a nondimensional strength factor.

Similitude requirements have been previously discussed by numerous authors including Kondner (1) and is repeated in this paper.

Frequently, tests that appear to be different because of different values of the physical quantities involved are in reality duplicate tests giving the same results when examined in nondimensional form. The reason for this is that in the search for an explicit relation expressing a physical phenomenon, it is the values of the nondimensional parameters, which are the new variables, that are important and not simply the magnitudes of the individual physical quantities. Thus, many of the results given by the field tests, conducted in a conventional dimensional form, are simply isolated parts or subspaces of the general nondimensional formulation (vector space).

MODEL DESIGN AND PRELIMINARY TESTS

Some of the important advantages of model tests vs field tests are that the former are more flexible, simpler to execute, relatively inexpensive and the variables are capable of more rigid control. They do however require correlation with field tests because unknown scale factors may be present which, if ignored, can lead to completely erroneous conclusions. Although the authors have formulated the functional relationships for the pole problem with both cohesive and cohesionless soils, it was considered advisable to conduct the initial experimental phase using sand rather than clay as the

soil medium for the following reasons. Sand properties are easier to control in the laboratory than those of clay and the time effects are generally considered to be less complex. Because good field test data on sand appears to be lacking, it was hoped that sometime later field tests could be conducted on sand using the model test results as a guide.

The model scale must be chosen so that the elements of the model can be easily manipulated (e.g., loads), and deflections simply measured.

Because the general pole problem containing both applied thrust and applied moment is quite difficult, it was decided to separate the two effects contained in Eq. 13; namely, the horizontal ground-line thrust F and the couple-moment at the ground-line M as follows:

$$\frac{y}{L} = \varkappa \left[\frac{C}{L}, \frac{C^2}{A}, \frac{F}{\gamma A L}, \frac{\gamma t C}{\eta}, \phi \right] \tag{14}$$

$$\frac{y}{L} = \varkappa \left[\frac{C}{L}, \frac{C^2}{A}, \frac{M}{\gamma A L^2}, \frac{\gamma t C}{\eta}, \phi \right] \tag{15}$$

By performing separate tests using (a) horizontal ground-line thrust only, (b) applied couple-moment only, and (c) thrust and bending moment combined; the data analysis can be simplified because in (a) and (b) the number of π-terms is reduced by one. Then from (a), (b), and (c) the principle of superposition can be checked. However, the scope of the model test study subsequently reported in this paper is confined to tests using a horizontal ground-line thrust only. A range in pole diameters of from ½ to 1½ in. and of embedments from 3 to 5½ in. was chosen. The couple-moment and combined studies are being conducted and will be reported in the future.

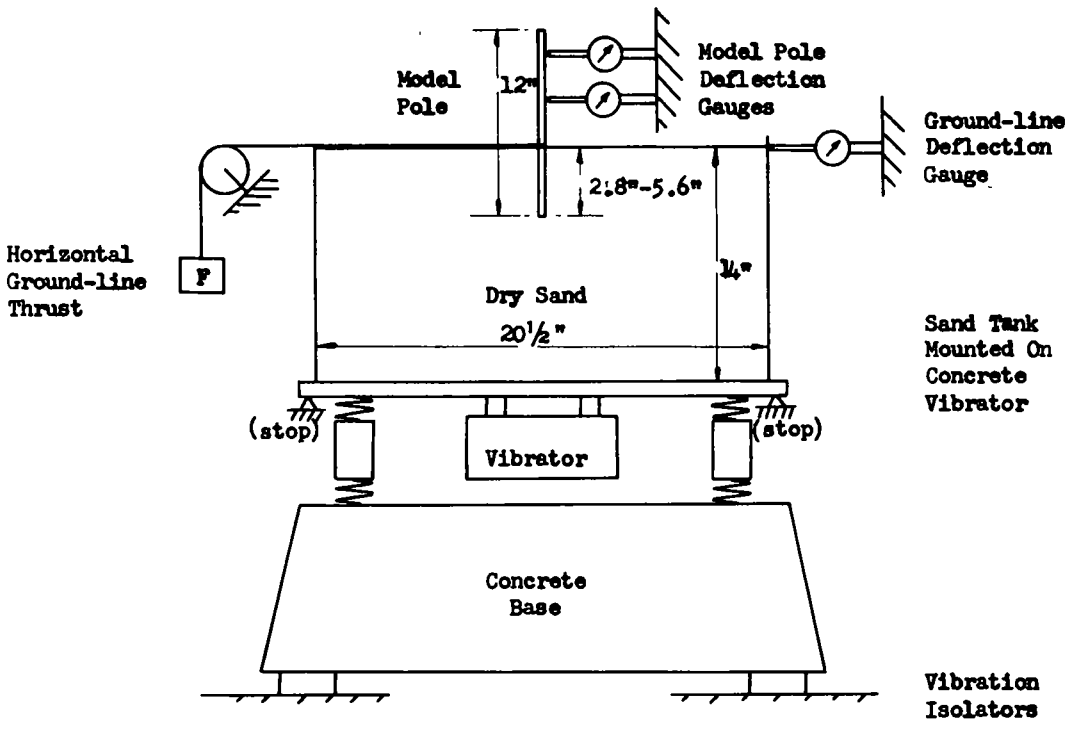

Figure 1. Model pole apparatus.

TABLE 2

PROPERTIES OF MODEL POLES

Pole No.	Material	Diameter (in.)	Area A (sq in.)	Weight (g)	Perimeter C (in.)
1	Aluminum	0.501	0.197	30	1.573
2	Aluminum	0.626	0.307	62	1.966
3	Steel	0.707	0.393	143	2.221
4	Steel	0.927	0.674	216	2.911
5	Steel	1.248	1.222	229	3.921
6	Steel	1.515	1.801	478	4.755

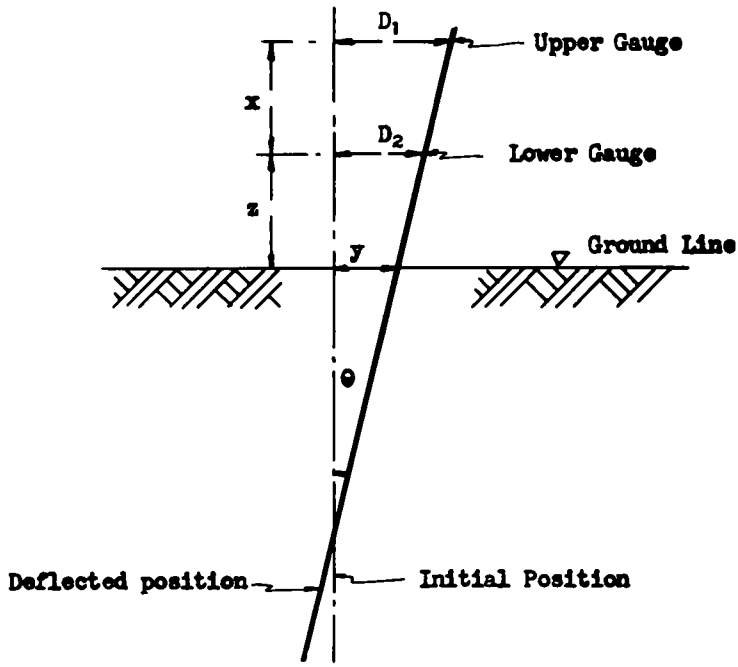

$$\frac{D_1 - D_2}{x} = \frac{D_2 - y}{z}$$

$$\therefore y = D_2 - \frac{z}{x}(D_1 - D_2)$$

if $x = z$

$$y = 2D_2 - D_1$$

Figure 2. Gauge set-up equation for ground-line deflection.

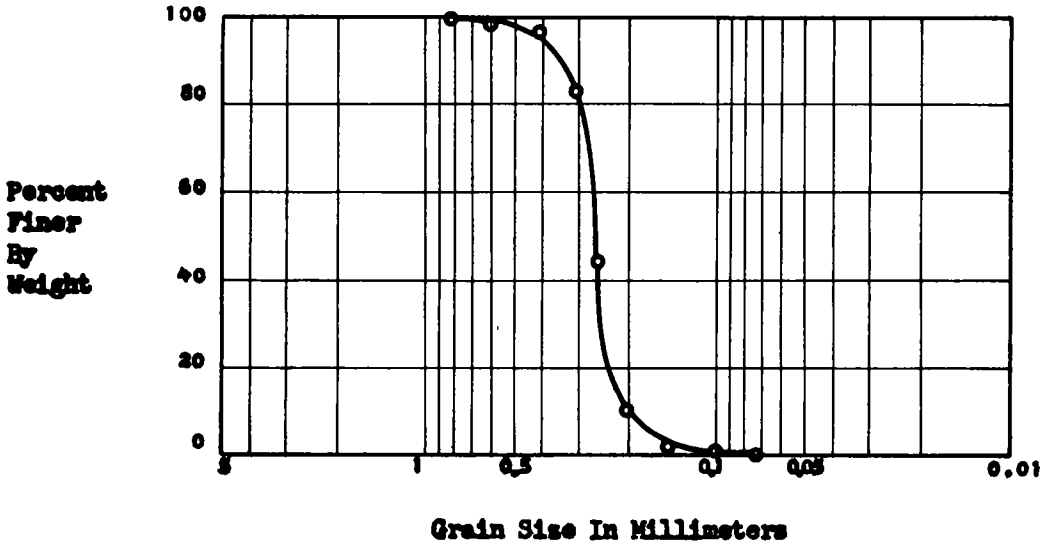

Figure 3. Grading curve for sand used in model.

The model pole apparatus used in the study is shown in Figure 1. A cut-down oil drum welded to a vibrating table-type concrete vibrator mounted on a heavy concrete base was used. To minimize the effect of building vibrations, the concrete base was supported on rubber blocks. The tank contained 330 lb of dry sand vibrated to as dense a state as possible. The model pole embedded in the sand was loaded by hanging weights on a cord attached to the pole at the ground-line and passing over a light pulley. The model poles consisted of 12-in. lengths of polished aluminum or steel tube, plugged at the lower end. Properties of these tubes are given in Table 2. The ground-line deflection of the pole was determined by measuring (a) the deflection at two points above ground level, from which the apparent ground-line deflection could be extrapolated, (see Fig. 2), and (b) a small correction due to the horizontal deflection of the tank relative to the two pole dial gauges. Gauges reading to 1/1, 000 in. were used for all tests except two where 1/10, 000-in. gauges were required. The sand used in the tank was a uniform fine dune sand from Wolf Lake, Ind., provided through the courtesy of the Raymond Concrete Pile Company, Chicago. The sand had a grading as shown in Figure 3 and was air-dried in the laboratory to a moisture content of about ¼ percent. For a dense state (i.e., density = 108 pcf) this sand had an angle of internal friction, ϕ, of 37°, as determined from a series of triaxial compression tests. Subsequent to extensive initial vibration the density of the sand in the tank remained constant at 107 pcf. The volume of the sand in the tank was determined from a calibration curve obtained by filling the tank with water and weighing it.

For the experimental data to be of any value the variables measured must truly represent the phenomena. Thus, in particular, the measured forces and deflections must be accurate.

It was found necessary to remove the springs from the pole dial gauges because the magnitude of the gauge spring force was high relative to the applied pole loads. The dial gauge arms were secured to the pole by elastic bands. It was also observed during the tests that the apparatus was very sensitive to vibrations transmitted to it through the floor. Heavy footsteps 3 to 4 ft away from the tank were sufficient to cause the dial gauge readings to "jump" a significant amount.

Because it was thought that the load rate might have a major effect on the shape of the load-deflection curve, similar tests under varying load rates were performed. The load rate was varied from 75 g per 2 min to 300 g per 2 min for constant C and L values in tests 4D, 4D/1, 4D/2, and 4D/3. The nondimensional plot of these data is shown

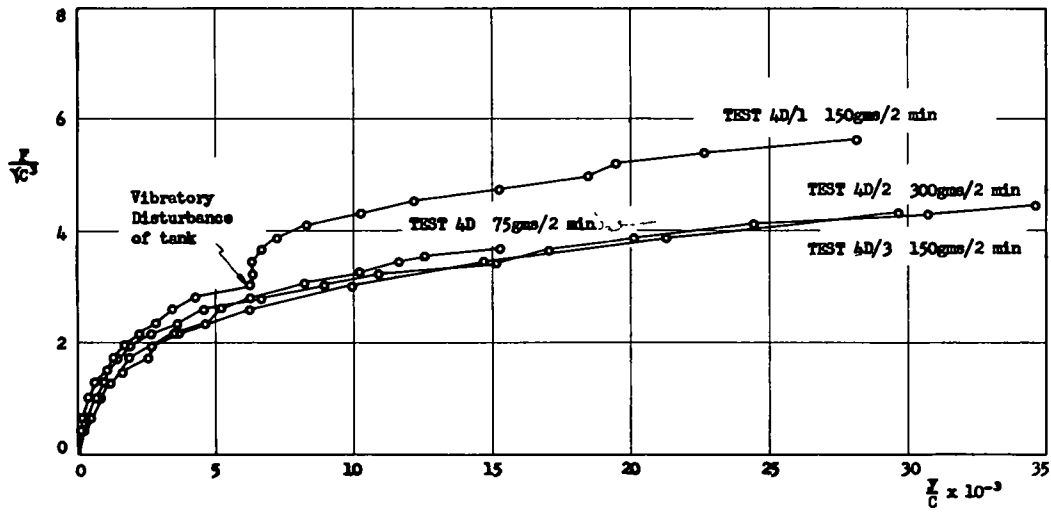

Figure 4. Nondimensional plot of $\frac{F}{\gamma C^3}$ versus $\frac{y}{C}$ for a constant value of $\frac{C}{L}$ = 0.6, for a varying load rate.

in Figure 4. The latter part of test 4D/1 was disturbed by accidental vibration of the tank. The three remaining curves for load rates of 75, 150, and 300 g per 2 min lie along the same line. This implies that, within this range, the rate of application of the load has no significant effect on the resulting $F/\gamma C^3$ vs y/C curves. Hence, although the value of the term $\gamma tC/\eta$ did not remain constant for the changing load rate, its influence was of little importance. Preliminary experiments suggested that the deflection under a given load increment was a time-dependent function; i.e., a creep phenomenon of some type. To investigate this, creep tests were conducted using 1/10,000-in. dial gauges instead of the normal 1/1,000-in. gauges used in all other tests. A typical result of such a creep test is shown in Figure 5. In this test, load increments of 75 g were applied at 5-min intervals until a total of 525 g was applied. Then on application of the next 75-g increment the deflections were measured at 1-min intervals for 15 min, whereupon 75 g increments were again applied at 5-min intervals up to a total of 900 g at which point a second 15-min creep test was performed. From the results of this and similar tests the following is concluded. When a load increment is applied, there is an initial sharp linear increase in deflection with time. After approximately 2 min, the slope of the line decreases sharply and the deflection continues at a much lower rate finally tending toward an ultimate value for a sufficiently large time. It was found that the slope of the upper part of the curve increases for an increase in applied load. Assuming that one need be concerned only with the initial deflections and can neglect the large time part of the deflection vs time curve, a load increment time interval of 2 min should prove satisfactory. Thus, load rate and creep tests indicate that the effects of the term $\gamma tC/\eta$ can be minimized.

TEST RESULTS

In using dimensional analysis to assist in interpreting the experimental data, one of the major problems is the choice of the exact form of the nondimensional groups. Because there are ten physical quantities and three fundamental units, the maximum number of dimensionless groups that can be obtained without considering powers is 210. Guided by previous work, experience, and preliminary results, a suitable form is selected. The effects of the variables must, if possible, be concentrated in individual π-terms so that phenomenological variations can be separated. The form of the nondimensional, functional relationship given by Eq. 14:

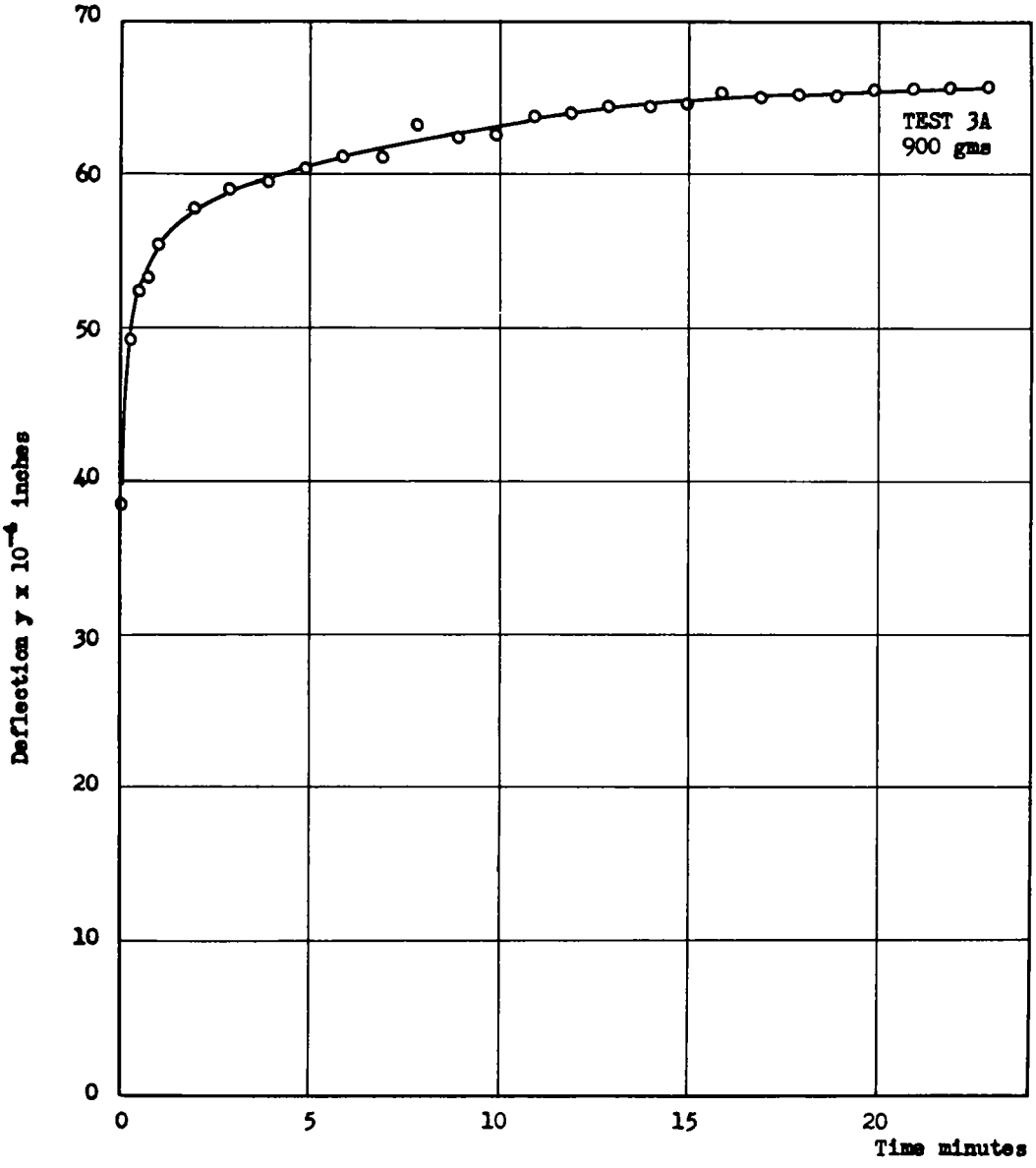

Figure 5. Plot of deflection y vs time for creep test, for a constant value of $\frac{C}{L} = 0.56$.

$$\frac{y}{L} = \varkappa\left[\frac{C}{L}, \frac{C^2}{A}, \frac{F}{\gamma AL}, \frac{\gamma tC}{\eta}, \phi\right] \tag{16}$$

can be algebraically transformed by forming the ratios

$$\frac{y/L}{C/L} = \frac{y}{C} \quad \text{and} \quad \frac{F/\gamma AL}{C/L.C^2/A} = \frac{F}{\gamma C^3}, \tag{17}$$

and replacing y/L and $F/\gamma AL$ to maintain independence of the π-terms. Thus, Eq. 16 may be rewritten

$$\frac{y}{C} = \varkappa\left[\frac{C}{L}, \frac{C^2}{A}, \frac{F}{\gamma C^3}, \frac{\gamma tC}{\eta}, \phi\right] \tag{18}$$

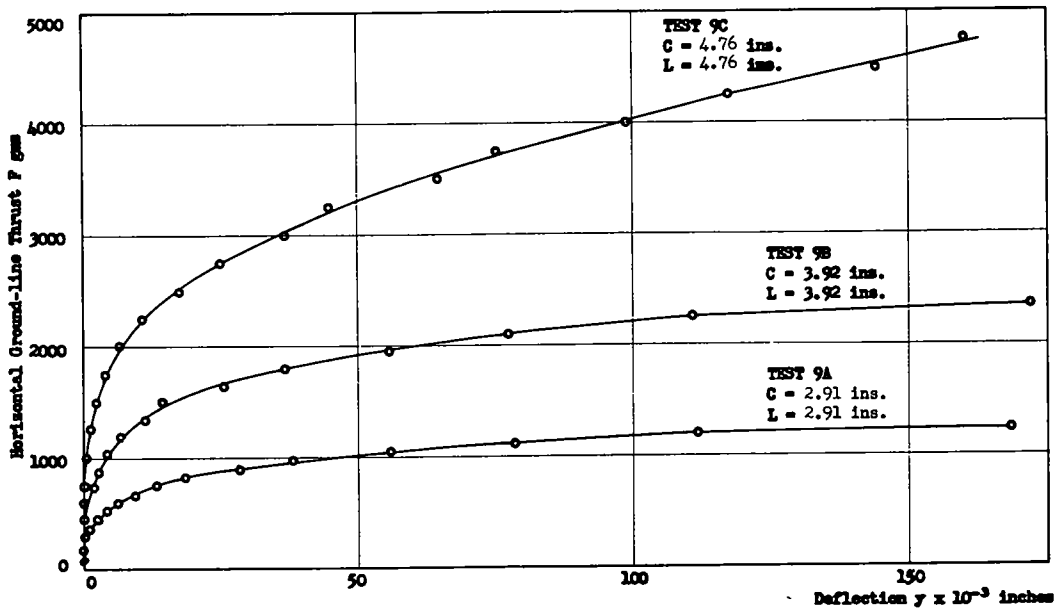

Figure 6. Plot of horizontal ground-line thrust F vs deflection y for a constant value of $\frac{C}{L} = 1.0$.

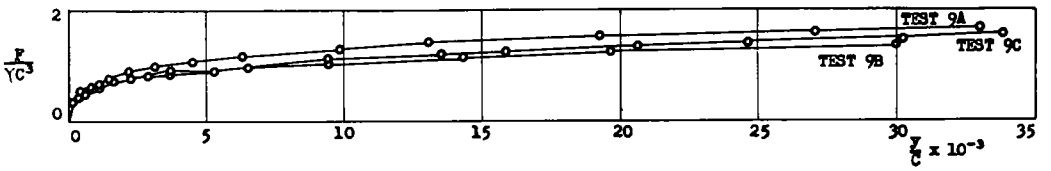

Figure 7. Nondimensional plot of $\frac{F}{\gamma C^3}$ vs $\frac{y}{C}$ for a constant value of $\frac{C}{L} = 1.0$.

In Eq. 18 the nondimensional term C^2/A is a constant equal to 4π for circular poles and its effect can be eliminated from the functional relationship because circular poles were used throughout the tests reported. The nondimensional term ϕ is a constant because the density, γ, of the sand is constant, and may also be eliminated from the functional relationship. It has been shown that the effects of the nondimensional term ytC/η can be minimized and therefore assumed to have a negligible influence on the function relationship. Hence, it may be eliminated. Thus, Eq. 18 may be rewritten

$$\frac{y}{C} = \varkappa\left[\frac{C}{L}, \frac{F}{\gamma C^3}\right] \tag{19}$$

To illustrate the advantages of presenting the experimental results in nondimensional form, data from Tests 9A, 9B, and 9C, for pole diameters of 0.927, 1.248, and 1.515 in. and embedded lengths of 2.91, 3.92, and 4.76 in. respectively were plotted in the conventional manner. Figure 6 is a plot of horizontal ground-line thrust F vs deflection y for the three tests. The seemingly important yet different influence of diameter and embedded length on the results are noteworthy. Because the C/L ratios for these three tests were constant, the data may also be plotted nondimensionally and reference to Figure 7 shows that they follow essentially the same curve.

An extensive program of tests were conducted for C/L values of 0.4, 0.6, 0.8, 1.0, and 1.2. The loading rate was varied to give approximately the same over-all time of

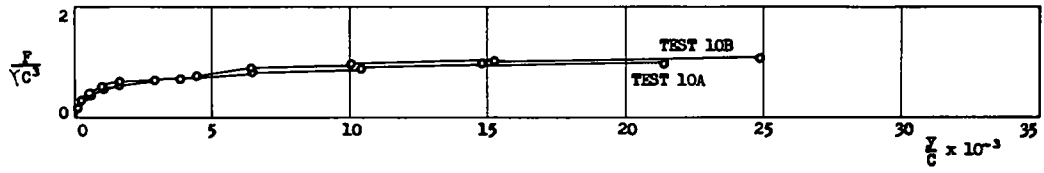

Figure 8. Nondimensional plot of $\frac{F}{\gamma C^3}$ vs $\frac{y}{C}$ for a constant value of $\frac{C}{L}$ = 1.2.

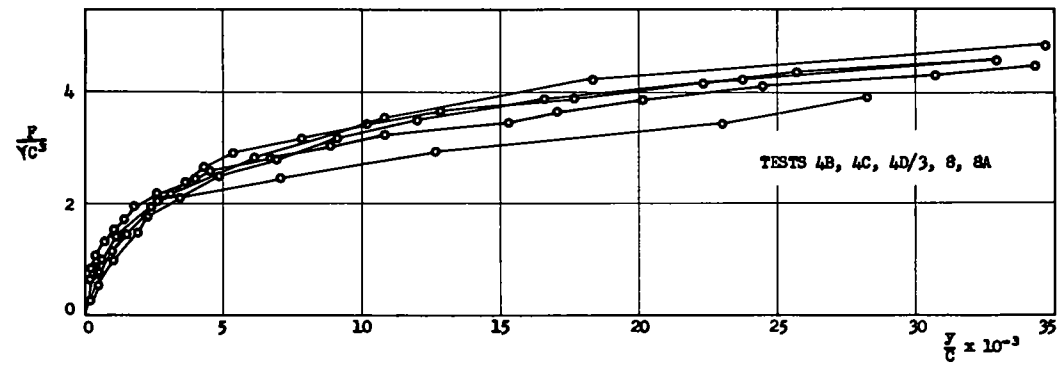

Figure 9. Nondimensional plot of $\frac{F}{\gamma C^3}$ vs $\frac{y}{C}$ for a constant value of $\frac{C}{L}$ = 0.6.

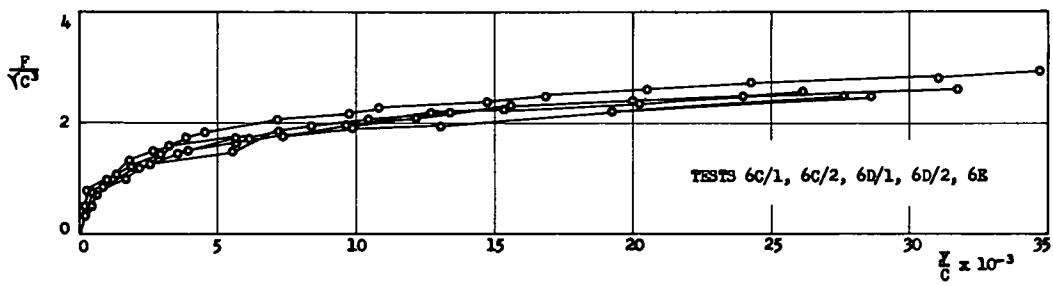

Figure 10. Nondimensional plot of $\frac{F}{\gamma C^3}$ vs $\frac{y}{C}$ for a constant value of $\frac{C}{L}$ = 0.8.

loading to failure in all tests. The nondimensional plots of these data appear in Figures 7 through 11 inclusive. In each test, a load increment was applied and the pole allowed to deflect, the gauge readings being recorded immediately before the application of the next load.

The maximum depth of embedment used in the tests was 5.6 in. For the plotted data the "scatter" is greatest for a C/L value of 0.4; i.e., for the smaller depths of embedment which exhibited the largest time effects. Figure 11 shows that this is true "scatter" and not a phenomenological difference. Thus, although tests 5A and 5A/1 were performed under apparently identical conditions their plots are different. As the C/L value increases from 0.4 to 1.2 the slight disparity between supposedly similar curves is reduced.

Although the load application rate was varied, the rate of stress application was not necessarily constant. In order to obtain a unique relationship between y/C, C/L and $F/\gamma C^3$ a constant value of $\gamma tC/n$ would have been required for the data included in each of Figures 7 through 11. Theoretically this could have been done by varying the loading

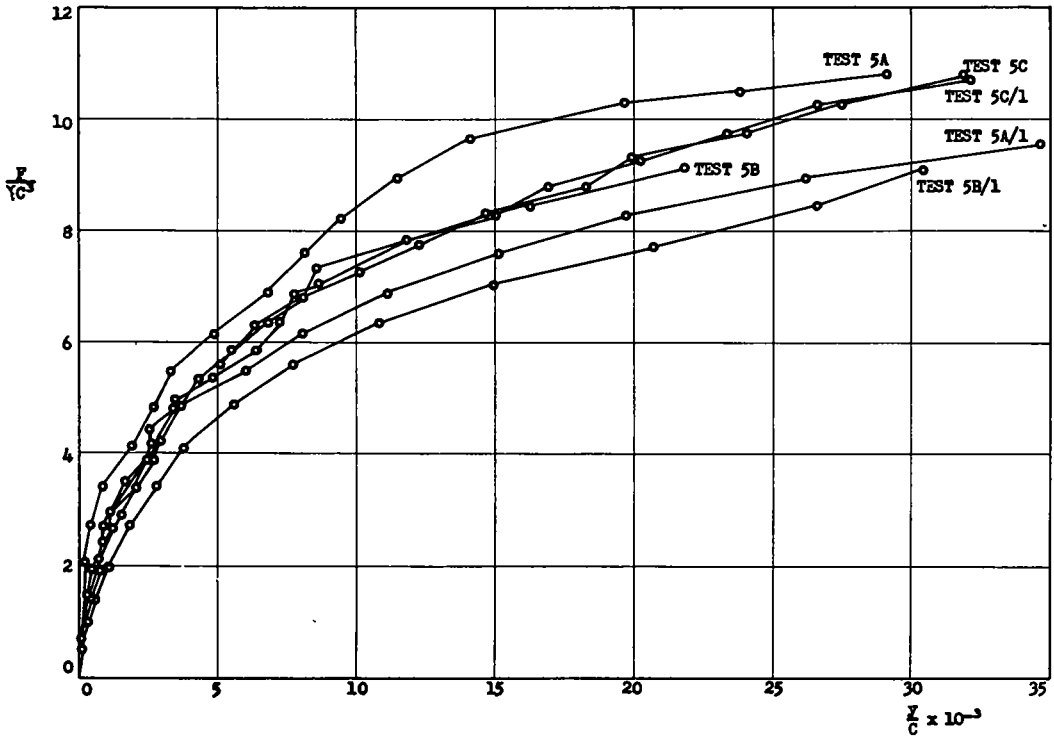

Figure 11. Nondimensional plot of $\frac{F}{\gamma C^3}$ vs $\frac{y}{C}$ for a constant value of $\frac{C}{L} = 0.4$.

rate for each test either by varying the load increment or by changing the time interval of loading. Unfortunately the field of soil mechanics has not yet reached a state of development where such loading rates can be predicted. Thus the "scatter" in the figures is probably due to time effects as well as experimental error, although as previously stated the effects of $\gamma tC/\eta$ were supposedly minimized.

If the soil is assumed to have failed when the angle of inclination θ of the pole with the vertical exceeds 5° (i.e., when $\tan\theta \geq 0.1$), Figure 2 shows, for x = z = 3 in., failure may be assumed to have occurred if

$$\tan\theta = \frac{D_1 - D_2}{3} \geq 0.1 \qquad (20)$$

i.e., if $D_1 - D_2 \geq 3,000 \times 10^{-4}$ in. because at no time did the difference in gauge readings exceed 0.3 in. one is justified in taking the whole of the $F/\gamma C^3$ vs y/C curve and basing a failure criterion on the asymptotic $F/\gamma C^3$ limit of the curve.

The shape of the thrust strength ratio vs deflection ratio curve is that of a nonlinear-type material. The curve tends asymptotically to an upper limit of the thrust strength ratio and had the load increment been reduced in this region it would have been possible to obtain higher points on the curve. However, the range of values actually covered is considered quite adequate. The nonlinearity of the thrust strength ratio vs deflection ratio indicates that the superposition principle is probably not valid. This would not agree with the use of a soil modulus approach. The degree of nonlinearity remains to be tested.

EXPLICIT FORM OF FUNCTIONAL RELATIONSHIP AND DEVELOPMENT OF NOMOGRAPHS

The experimental data plotted in Figures 7 through 11 in nondimensional form were used to develop an empirical relationship relating the three π-terms of Eq. 19. Mean curves were drawn through the experimental curves and appear in Figure 12. By replotting these mean curves on a semi-logarithmic scale, near straight lines were obtained as shown in Figure 13. The curves were further straightened out by replotting in the form log $(y/C + \bar{A})$ vs $F/\gamma C^3$, as shown in Figure 14, to give a two-constant curve of the type

$$\frac{y}{C} = \bar{A}\left[e^{B\frac{F}{\gamma C^3}} - 1\right] \tag{21}$$

in which $\bar{A}$ and B are constants. The value of $\bar{A}$ is given by the intercept of the line on the log $(y/C + \bar{A})$ axis for $F/\gamma C^3 = 0$. By plotting values of this intercept against C/L an equation relating $\bar{A}$ and C/L was found:

$$\bar{A} = 0.7 - 0.5\frac{C}{L} \tag{22}$$

A plot of this data appears in Figure 15.

By plotting values of the slope of the lines in Figure 14 (the constant B) against C/L on a logarithmic scale as shown in Figure 16, an equation relating B and C/L was found:

$$B = 3.28\left(\frac{C}{L}\right)^{-2.24} \tag{23}$$

Therefore, the empirical equation relating the three π-terms $F/\gamma C^3$, y/C, and C/L may be written:

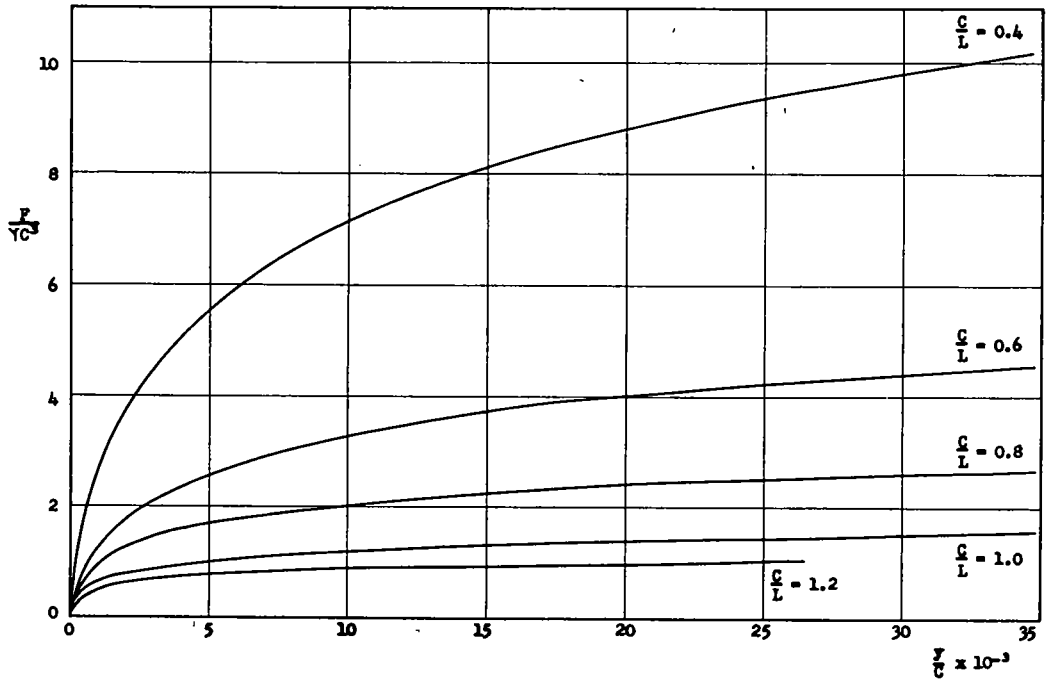

Figure 12. Nondimensional plot of $\frac{F}{\gamma C^3}$ vs $\frac{y}{C}$ mean curves to experimental data for $\frac{C}{L}$ = 0.4 - 1.2.

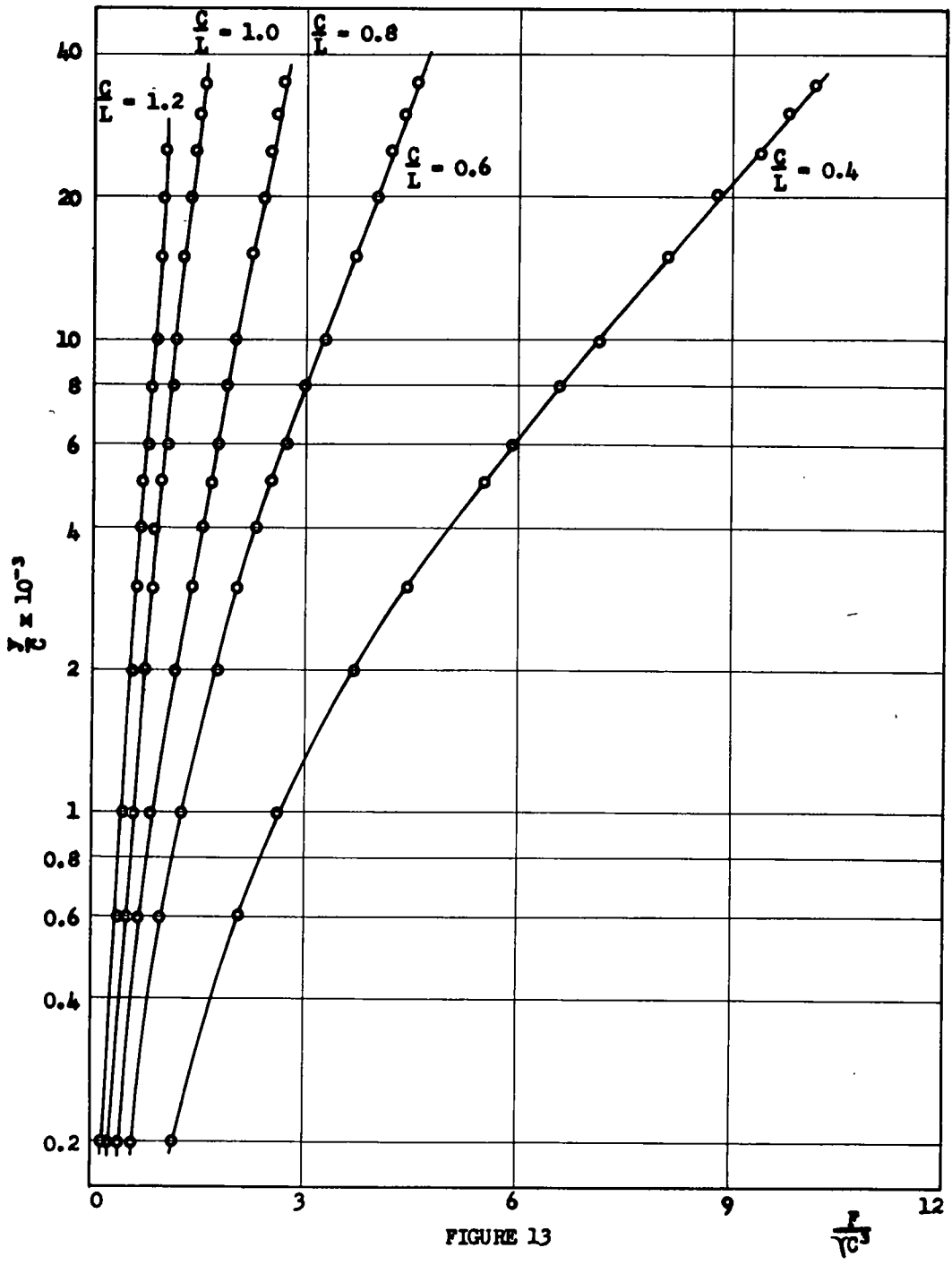

Figure 13. Nondimensional plot of $\frac{F}{\gamma C^3}$ vs $\frac{Y}{C}$ mean curves to experimental data for $\frac{C}{L}$ = 0.4 - 1.2.

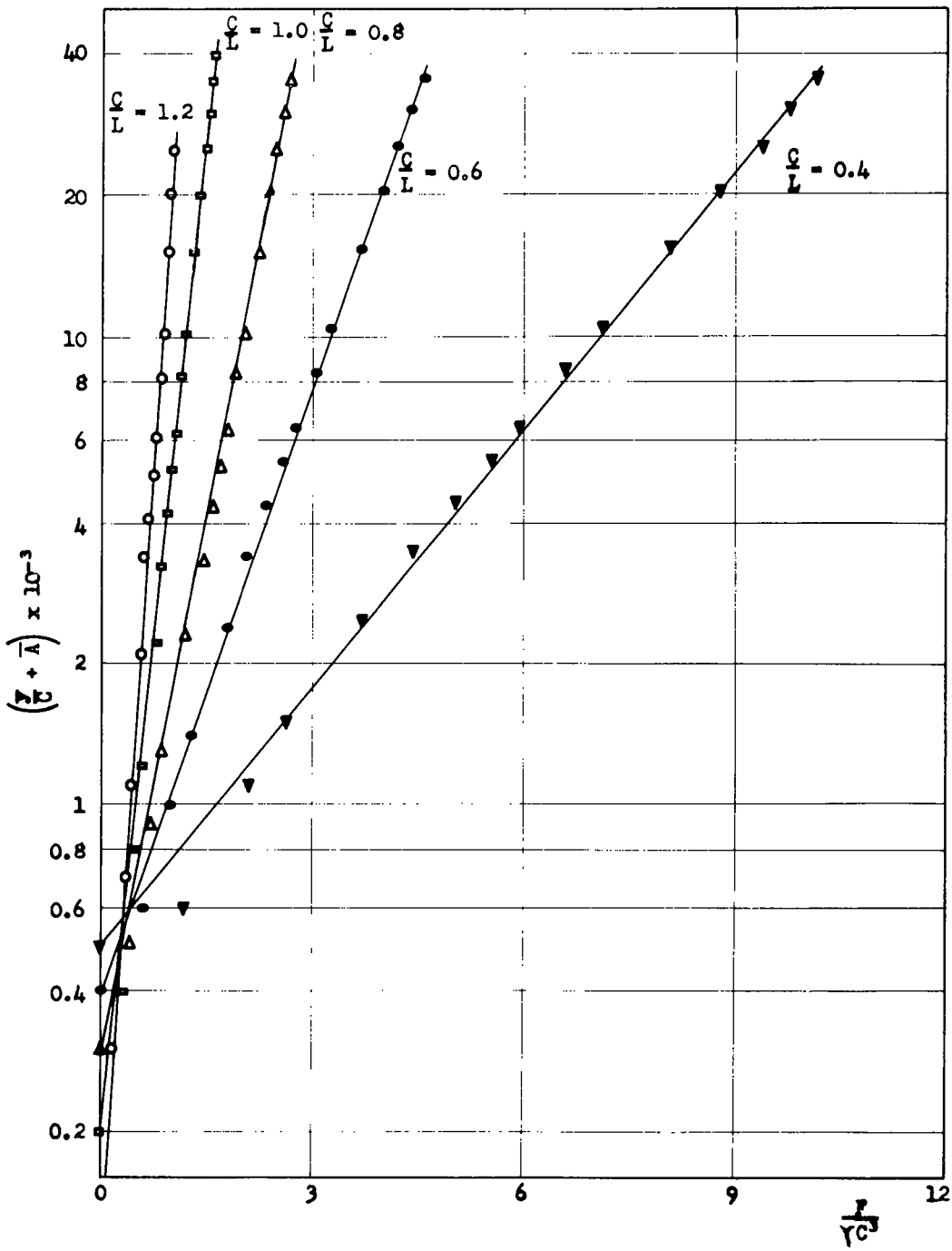

Figure 14. Nondimensional plot of $\frac{F}{\gamma C^3}$ vs $\left[\frac{y}{C} + \bar{A}\right]$ mean curves to experimental data for $\frac{C}{L} = 0.4 - 1.2$.

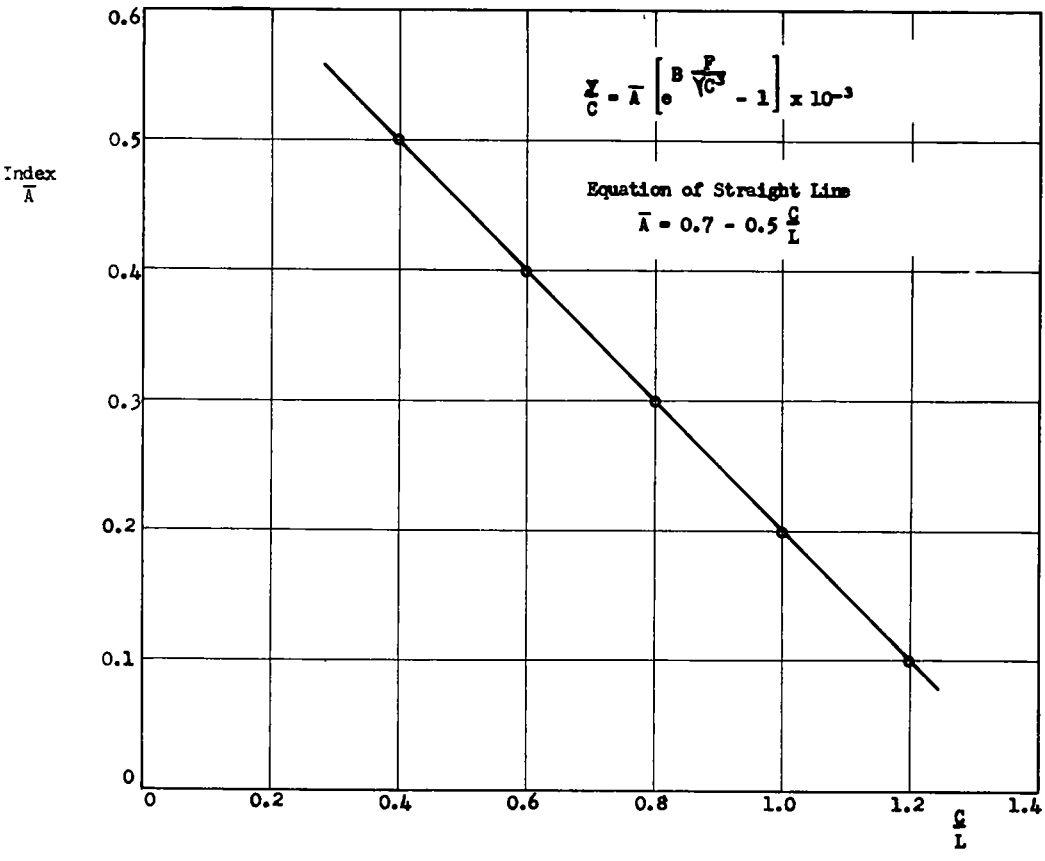

Figure 15. Plot of index $\bar{A}$ vs $\frac{C}{L}$.

$$\frac{y}{C} = \left(0.7 - 0.5\frac{C}{L}\right)\left[e^{3.28\left(\frac{C}{L}\right)^{2.24}\frac{F}{\gamma C^3}} - 1\right] \times 10^{-3} \qquad (24)$$

Alternatively Eq. 24 may be rewritten to give $F/\gamma C^3$ in terms of y/C and C/L:

$$\frac{F}{\gamma C^3} = 0.70\left(\frac{C}{L}\right)^{-2.24} \log_{10}\left[\frac{\frac{y}{C} \times 10^3}{0.7 - 0.5\frac{C}{L}} + 1\right] \qquad (25)$$

A nomograph for Eqs. 24 and 25 has been computed and appears in Figure 17. The five curves are almost identical with the mean curves of Figure 12, indicating satisfactory curve fitting. Although Eqs. 24 and 25 and Figure 17 only apply for values of y/C up to approximately 50×10^{-3}, the complete practical range is included since $y/C = 50 \times 10^{-3}$ is well in the range of failure or instability.

In an effort to develop an equation for the ultimate strength ratio, independent of the deflection ratio; a graph of the ultimate value of $F/\gamma C^3$ vs C/L was plotted in Figure 18. For values of C/L less than about 0.4, the curve tends asymptotically to infinity and the pole becomes a flexible pile. According to Czerniak (8) a pole is a pile "whose embedded depth does not exceed ten times its least lateral dimension." For a C/L value of

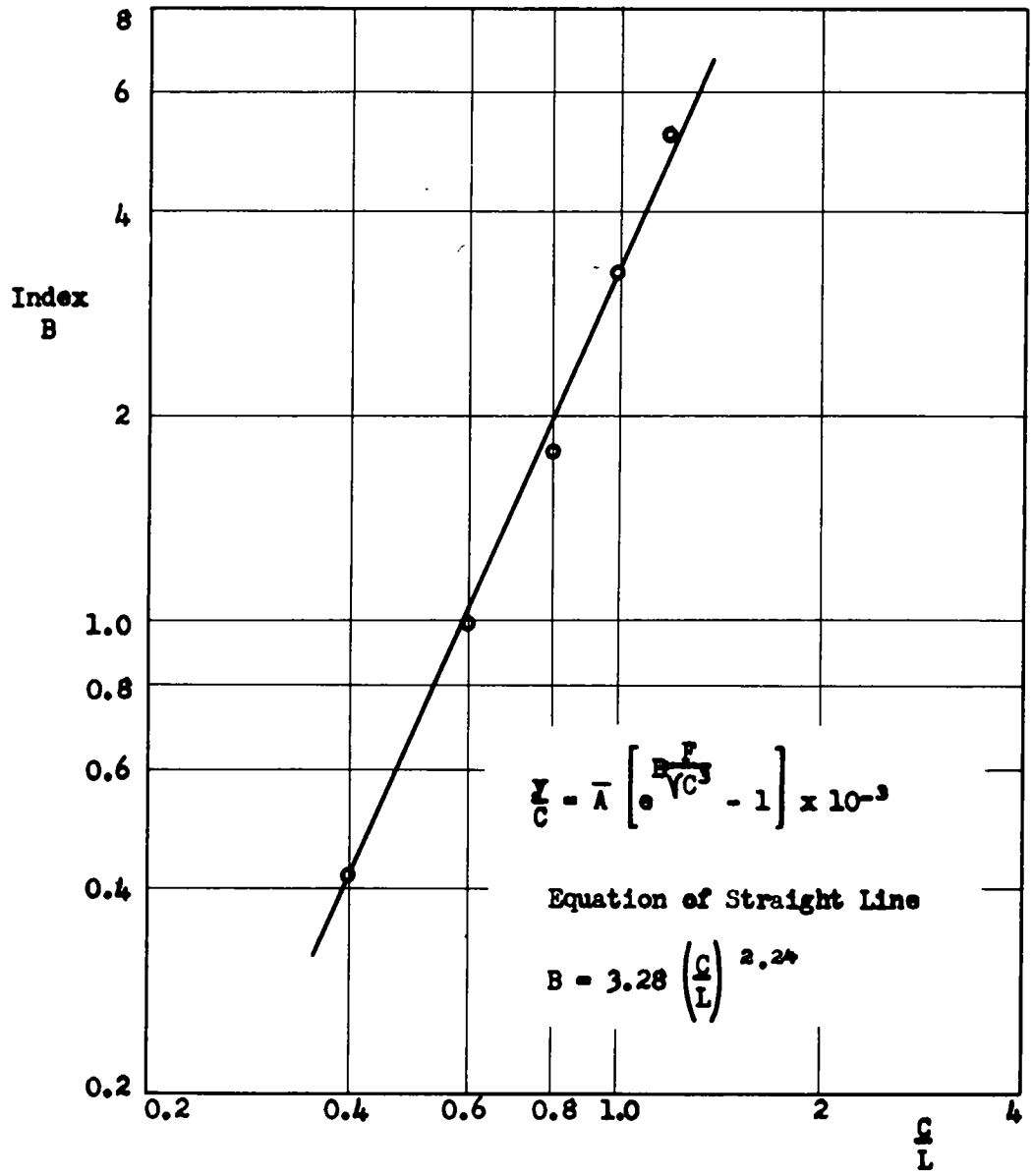

Figure 16. Plot of index B vs $\frac{C}{L}$.

0.4, the embedded length is 7.5 times the diameter. This is a relatively crude working rule inasmuch as no account is taken of the moment of inertia of the pole. Matlock and Reese (10) introduce the concept of a "maximum depth coefficient" to define a pile-pole criterion. This coefficient is related to the stiffness of the pile but is of such a complex nature that it appears to be difficult to relate it to the pole-soil interaction under investigation. This discussion of C/L is not an attempt to define a pole or pile, but is only intended as a qualitative discussion of the seemingly asymptotic nature for the small and large values of C/L given in Figure 18.

For values of C/L greater than 1.5 or 2, the strength ratio is very small and the resistance to deformation becomes very small. This corresponds to the case of a

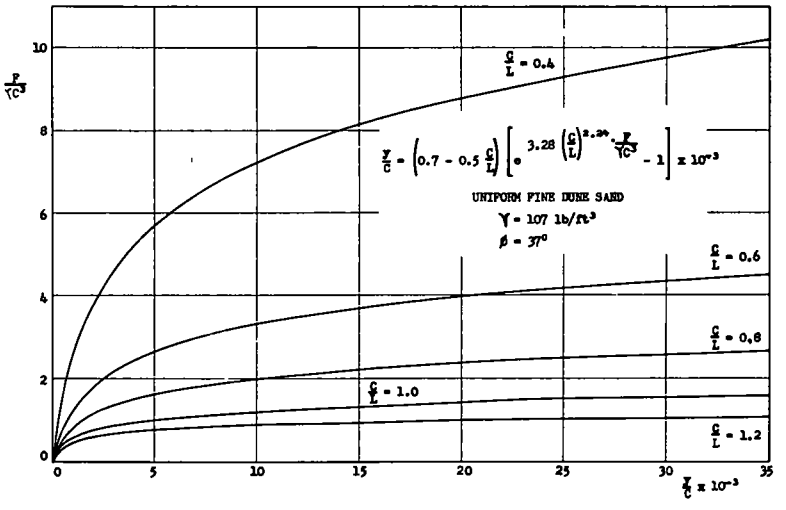

Figure 17. Nomograph relating $\frac{F}{\sqrt{C^3}}$, $\frac{Y}{C}$, and $\frac{C}{L}$.

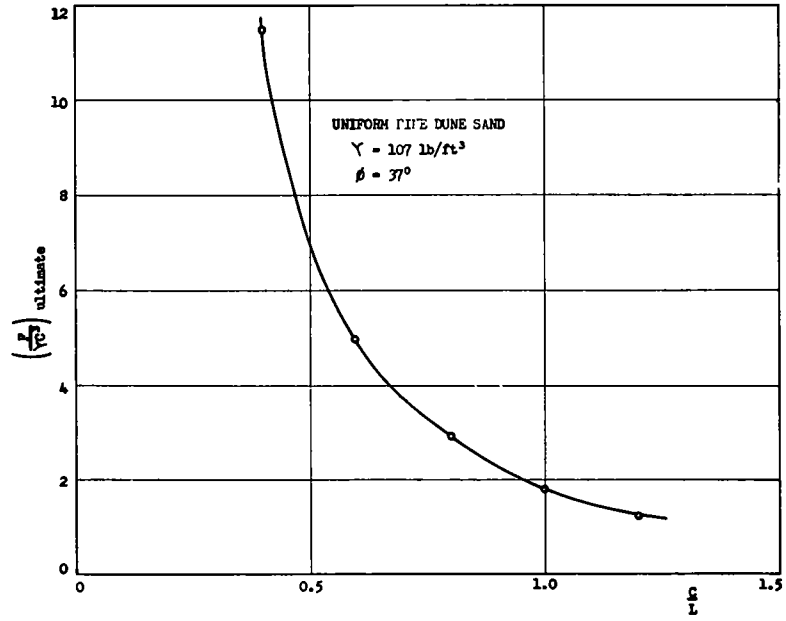

Figure 18. Plot of $\left(\frac{F}{\sqrt{C^3}}\right)$ ultimate vs $\frac{C}{L}$.

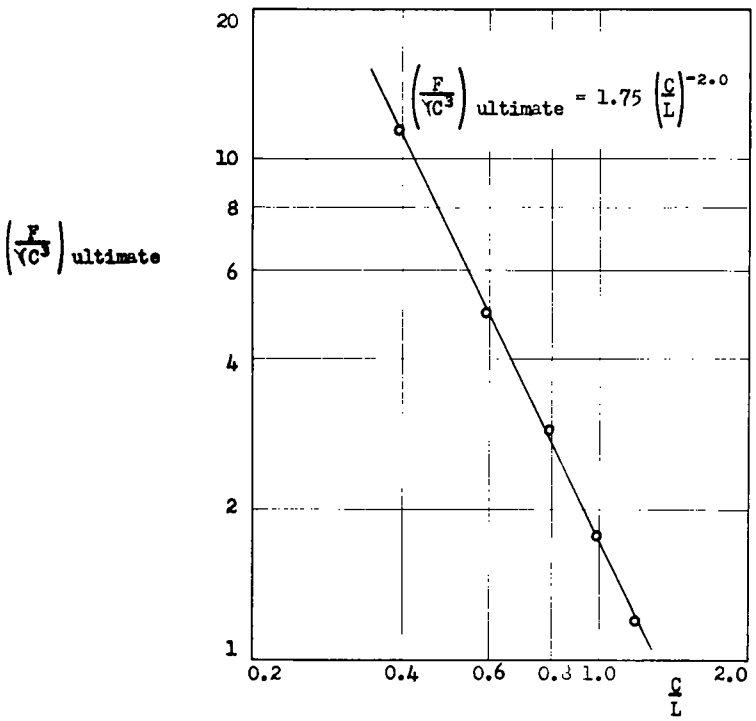

Figure 19. Plot of $\left(\frac{F}{\gamma C^3}\right)$ ultimate vs $\frac{C}{L}$.

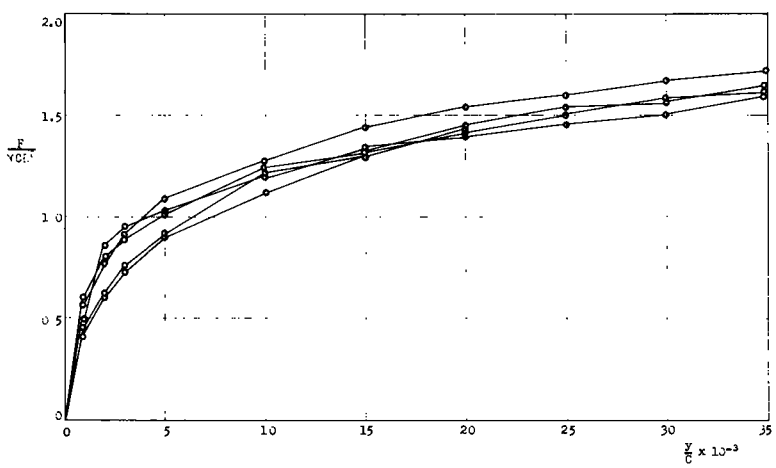

Figure 20. Nondimensional plot of $\frac{F}{\gamma CL^2}$ vs $\frac{V}{C}$ for $\frac{C}{L}$ = 0.4 - 1.2.

footing, with a horizontal applied load, in which the vertical forces, both body and applied, are very small and hence the frictional resistance is very small.

By replotting the data of Figure 18 on a logarithmic scale a straight line was obtained, the equation of which was

$$\left(\frac{F}{\gamma C^3}\right)_{\text{ultimate}} = 1.75 \left(\frac{C}{L}\right)^{-2} \tag{26}$$

which may be written

$$\left(\frac{F}{\gamma CL^2}\right)_{\text{ultimate}} = 1.75 \tag{27}$$

in which $F/\gamma CL^2$ is a stability number for the pole problem under consideration. A plot of these data appears in Figure 19. The empirical Eq. 27 is relatively simple and gives the ultimate ground-line thrust, F, directly.

The nondimensional form of Eq. 27 suggests a more optimum form for the functional relationship given by Eq. 19. This can be obtained by multiplying $F/\gamma C^3$ by $(C/L)^2$ to get the new term $F/\gamma CL^2$ and by dropping $F/\gamma C^3$ to maintain independence. Thus,

$$\frac{y}{C} = \varkappa \left[\frac{F}{\gamma CL^2} , \frac{C}{L} \right] \tag{28}$$

The mean curves to the experimental data previously given have been replotted in the form of $F/\gamma CL^2$ vs y/C for a range of C/L varying from 0.4 to 1.2 in Figure 20. Although the functional form of Eq. 19, as plotted in Figure 12, indicates a dependence on C/L, the form given by Eq. 28 and shown in Figure 20 indicates that the effects of the depth of embedment have been "lumped" into the term $F/\gamma CL^2$ and, except for experimental error, C/L has a negligible influence on the results. This permits the obtaining of a simpler, although more approximate, equation relating the variables of Eq. 28. Considering the mean curve to be independent of C/L, Eq. 19 may be rewritten:

$$\frac{y}{C} = \varkappa \left[\frac{F}{\gamma CL^2} \right] \tag{29}$$

in which the effect of C/L is negligible and may therefore be eliminated.

By replotting the curves on a semi-logarithmic scale, a near straight line was obtained as shown in Figure 21. The curve was further straightened out by replotting in the form log (y/C + A') vs $F/\gamma CL^2$, as shown in Figure 22, to give a two-constant curve, whose equation was

$$\frac{y}{C} = 0.2 \left(e^{3.20 \frac{F}{\gamma CL^2}} - 1 \right) \tag{30}$$

The value of A' is given by the intercept of the line on the log (y/C + A') axis for $F/\gamma CL^2 = 0$.

Alternatively Eq. 30 may be rewritten to give $F/\gamma CL^2$ in terms of y/C:

$$\frac{F}{\gamma CL^2} = 0.72 \log_{(10)} \left[5{,}000 \frac{y}{C} + 1 \right] \tag{31}$$

A nomograph for Eqs. 30 and 31 has been computed and appears in Figure 23. The curve is almost identical to a mean curve of Figure 20 indicating satisfactory curve fitting.

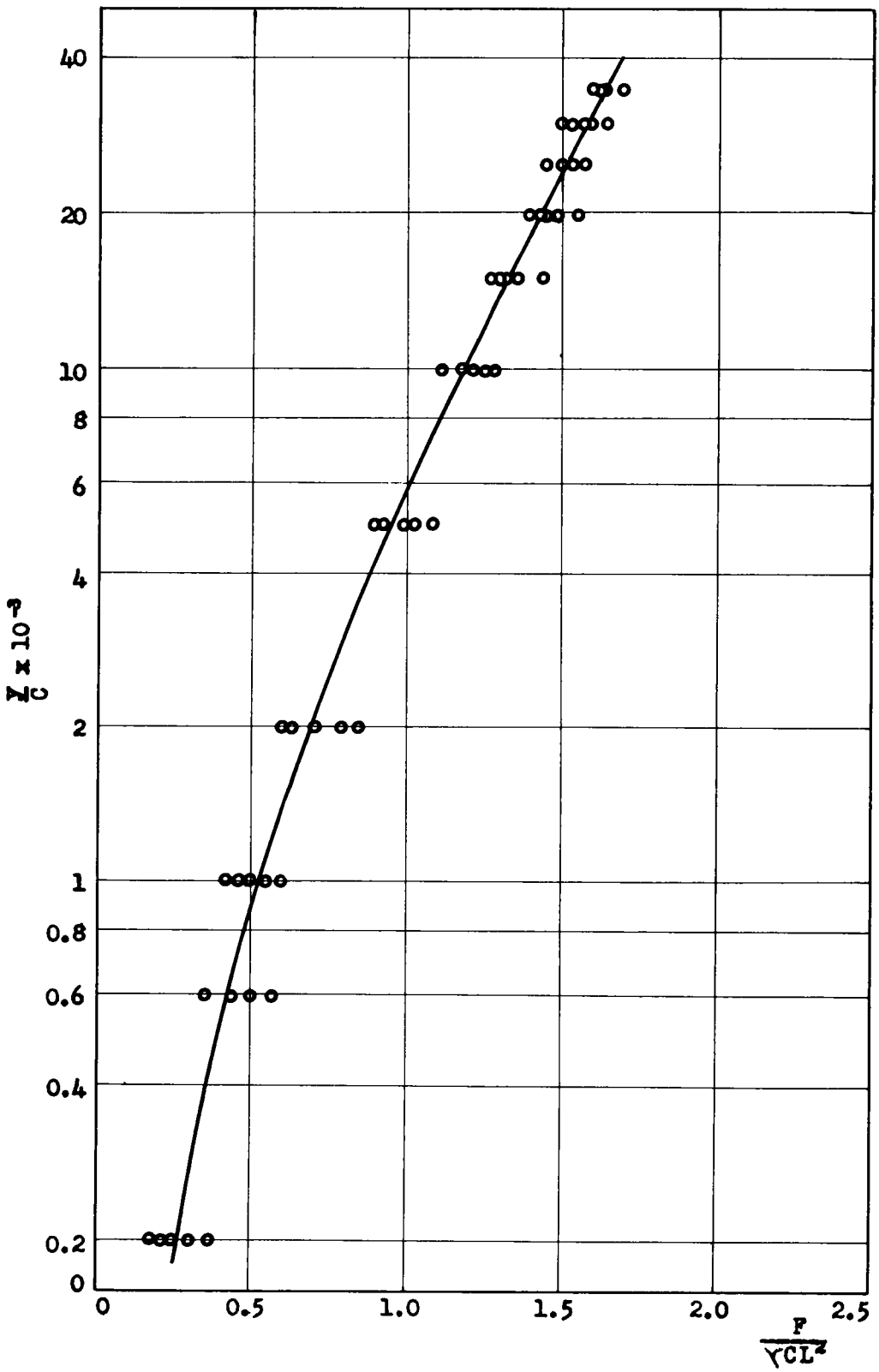

Figure 21. Nondimensional plot of $\frac{F}{\gamma CL^2}$ vs $\frac{y}{C}$ for $\frac{C}{L}$ = 0.4 - 1.2.

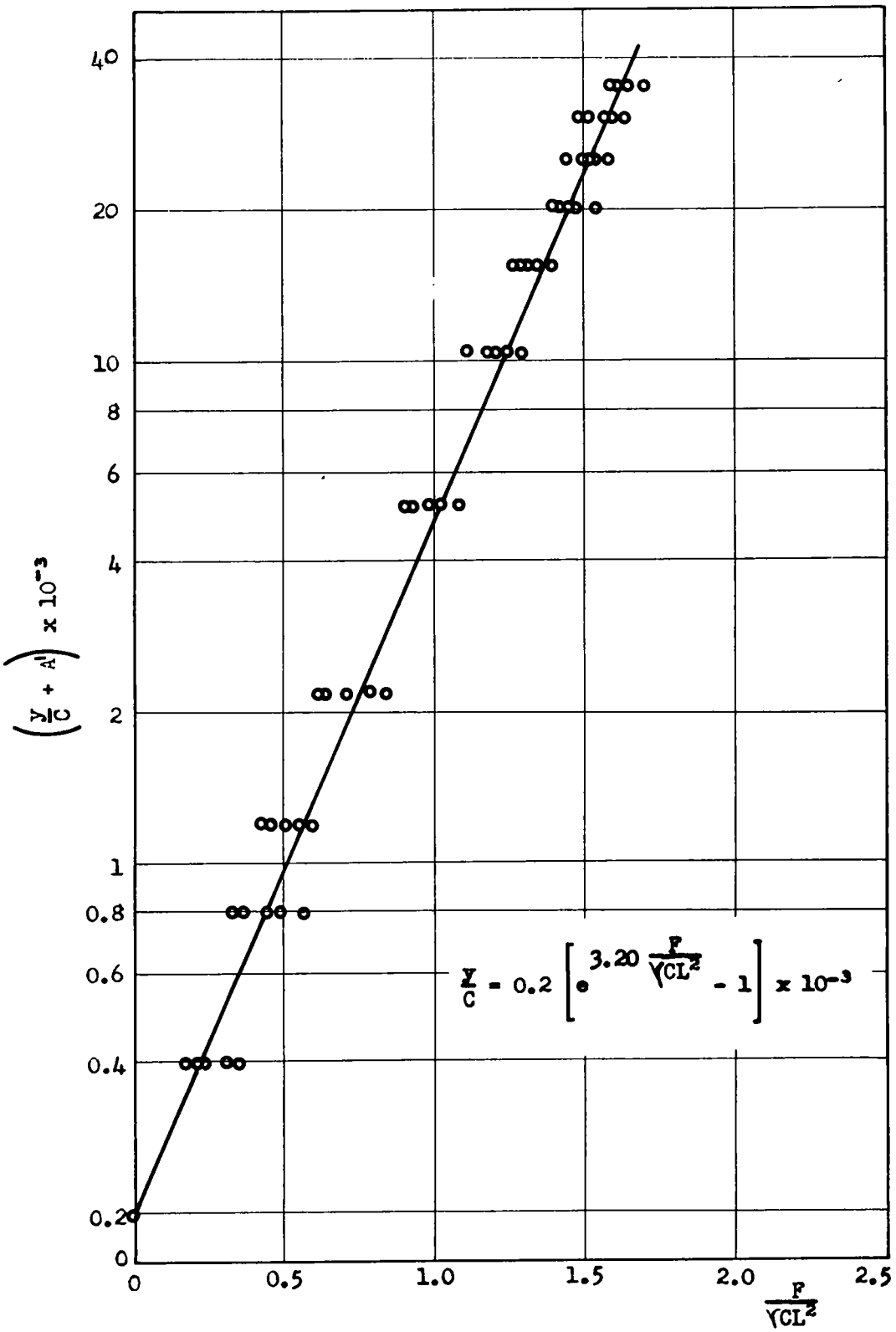

Figure 22. Nondimensional plot of $\frac{F}{\gamma CL^2}$ vs $\left(\frac{y}{C} + A'\right)$ for $\frac{C}{L}$ = 0.4 - 1.2.

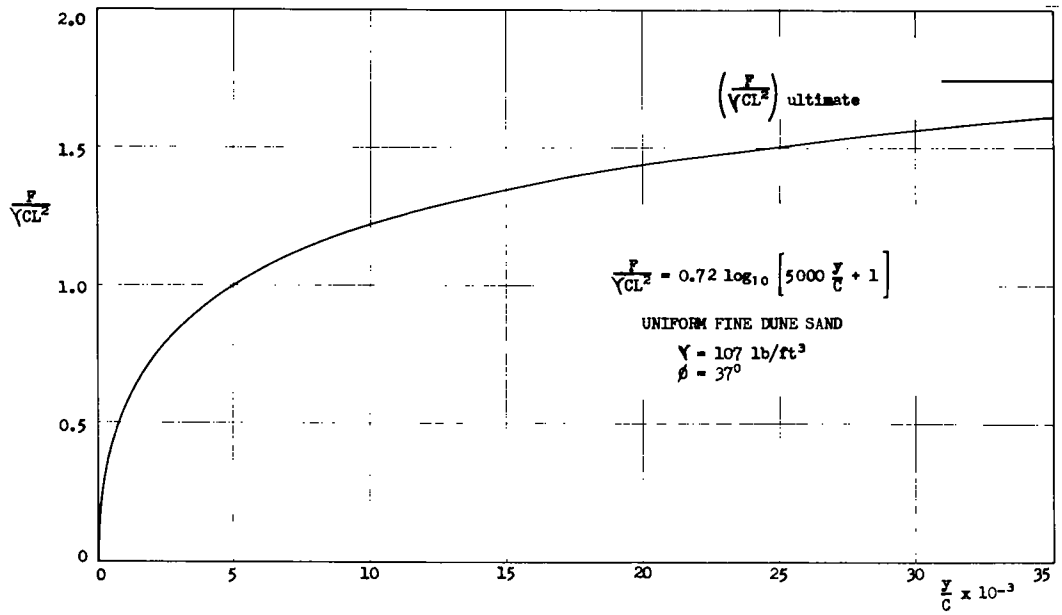

Figure 23. Nomograph relating $\frac{F}{\gamma CL^2}$ and $\frac{y}{C}$.

Referring to Figure 12, the maximum values of $F/\gamma C^3$ occur for a value of y/C of approximately 50 x 10^{-3}. Substituting this into Eq. 31 gives

$$\frac{F}{\gamma CL^2} = 0.72 \log 251 = 1.75 \qquad (32)$$

which is identical with Eq. 27, obtained by considering the ultimate values only. From this it may be inferred that the mathematical forms of Eqs. 27, 30, and 31 are compatible with one another.

In summary, although the general functional relationship for the problem has been developed, this paper deals primarily with the horizontal ground-line thrust on a pole embedded vertically in a uniform fine sand. The effects of pure couple-moments and superposition for both clays and sands are being investigated as well as the effects of soil type, density, and consistency. It is hoped that full-scale tests will be conducted in the future to correlate field response with the model study. The following examples are given to show the possible use to which model results may some day be applicable.

EXAMPLES

In the first example it has been assumed that the model test results may be applied directly to a field prototype so as to determine the order of magnitude of the field test results.

Given: A 10 ¾-in. circular steel pole was embedded in a uniform fine dune sand, density 107 pcf, $\phi = 37°$, and was subjected to a horizontal ground-line thrust.

Required: (a) The ultimate load for an embedment of 4 ft 6 in.
(b) The factor of safety for an applied load of 3 tons.
(c) The ground-line deflection in (b).
(d) An estimate of the ultimate deflection in (a).

Solution: $C = 10\ ¾ \times \pi = 33.8$ in. $= 2.82$ ft
$L = 54$ in. $= 4.5$ ft
$\frac{C}{L} = 0.63$

(a) From Figure 18,

$$\text{for } \frac{C}{L} = 0.63; \left[\frac{F}{\gamma C^3}\right]_{\text{ultimate}} = 4.45,$$

$$F_{\text{ultimate}} = 4.45\,\gamma C^3$$

$$= 4.45 \times \frac{107}{2000} \times (2.82)^3$$

$$= 5.35 \text{ tons}$$

Alternatively, using the pole stability number of Eq. 27

$$\left[\frac{F}{\gamma CL^2}\right]_{\text{ultimate}} = 1.75$$

$$F_{\text{ultimate}} = 1.75\,\gamma CL^2 = 1.75 \times \frac{107}{2000} \times 2.82 \times (4.5)^2$$

$$= 5.35 \text{ tons}$$

(b) Factor of safety $= \frac{5.35}{3} = 1.78$

(c) $$\frac{F}{\gamma CL^2} = \frac{3 \times 2000}{107 \times 2.82 \times (4.5)^2} = 0.98$$

from Figure 23

$$\text{for } \frac{F}{\gamma CL^2} = 0.98\ ;\ \frac{y}{C} = 4.7 \times 10^{-3}$$

$$\therefore\ y = 4.7 \times 33.8 \times 10^{-3} = 0.16 \text{ in.}$$

Alternatively,

$$\frac{F}{\gamma C^3} = \frac{3 \times 2000}{107 \times 2.82^3} = 2.50$$

from Figure 17

$$\text{for } \frac{F}{\gamma C^3} = 2.50\ ;\ \frac{C}{L} = 0.63\ ;\ \frac{y}{C} = 4.7 \times 10^{-3}$$

$$\therefore\ y = 0.16 \text{ in. (as before)}$$

(d) an estimate of the ultimate deflection may be determined from

$$\left(\frac{y}{C}\right)_{\text{ultimate}} \approx 50 \times 10^{-3}$$

$$y_{\text{ultimate}} \approx 50 \times 33.8 \times 10^{-3}$$

$$\approx 1.70 \text{ in.}$$

The first example could have been presented as a design problem rather than one of analysis.

Given: A 10 ¾-in. circular steel pole is to be embedded in a uniform fine dune sand, density 107 pcf, $\phi = 37^\circ$, and subjected to a horizontal ground-line thrust of 3.0 tons.

Required: (a) The depth of embedment for a factor of safety of 1.78 against failure.
(b) The ground-line deflection in (a).

Solution: $C = 10\ \frac{3}{4} \times \pi = 2.82 \text{ ft} = 33.8 \text{ in.}$

$$F_{\text{design}} = 1.78 \times 3 = 5.35 = F_{\text{ultimate}}$$

(a) from Figure 18

$$\text{for}\left[\frac{F}{\gamma C^3}\right]_{\text{ultimate}} = \frac{5.35 \times 2000}{107 \times (2.82)^3} = 4.45$$

$$\frac{C}{L} = 0.63$$

$$\text{Therefore, } L = \frac{C}{0.63} = \frac{2.82}{0.63} = 4.5 \text{ ft}$$

Alternatively, use of the pole stability number of Eq. 27 gives

$$\left[\frac{F}{\gamma CL^2}\right]_{\text{ultimate}} = 1.75$$

$$L = \sqrt{\frac{F_{\text{ultimate}}}{1.75\gamma C}} = \sqrt{\frac{5.35 \times 2,000}{1.75 \times 107 \times 2.82}} = 4.5 \text{ ft}$$

(b) from Figure 23

$$\text{for } \frac{F}{\gamma CL^2} = 0.98$$

$$\frac{y}{C} = 4.7 \times 10^{-3}$$

Therefore, $y = 4.7 \times 33.8 \times 10^{-3} = 0.16$ in.

CONCLUSIONS

1. For a model pole embedded in a very dense sand having constant properties the following theoretical, functional relationship has been developed to describe the phenomena:

$$\frac{y}{L} = \varkappa\left[\frac{C}{L}, \frac{C^2}{A}, \frac{M}{\gamma AL^2}, \frac{F}{\gamma AL}, \frac{\gamma tC}{n}, \phi\right] \tag{13}$$

2. For a model pole embedded vertically in a very dense uniform fine dune sand, density 107 pcf and angle of internal friction 37°, subject to a horizontal ground-line thrust:

(a) Variation in the diameter and depth of embedment of the pole resulted in different load-deflection curves. When the data were then plotted non-dimensionally in terms of $F/\gamma C^3$ vs y/C, a series of curves for differing C/L values resulted. These could be further approximated to a single curve for $F/\gamma CL^2$ vs y/C.

(b) A series of nomographs were constructed giving: 1. A relationship between the thrust strength ratio, $F/\gamma C^3$; the deflection ratio, y/C; and the slenderness ratio, C/L:

$$\frac{F}{\gamma C^3} = 0.70\left(\frac{C}{L}\right)^{-2.24} \log_{10}\left[\frac{\frac{y}{C} \times 10^3}{0.7 - 0.5\frac{C}{L}} + 1\right] \tag{25}$$

2. A slightly simplified, but more approximate, relationship between a "modified" thrust strength ratio, $F/\gamma CL^2$; and the deflection ratio, y/C:

$$\frac{F}{\gamma CL^2} = 0.72 \log_{10}\left[5,000\frac{y}{C} + 1\right] \tag{31}$$

3. A failure criterion relating the ultimate thrust strength ratio, $(F/\gamma C^3)_{\text{ultimate}}$; and the slenderness ratio, C/L; which may be written in the form of a stability number:

$$\left(\frac{F}{\gamma CL^2}\right)_{\text{ultimate}} = 1.75 \tag{27}$$

3. The use of dimensional analysis in interpreting the data permits the reducing of them to a relatively simple form, for which empirical equations may be developed. Conventional methods result in numerous disconnected "bits" of information.

4. Because there have been no field tests to correlate with the model study, caution is recommended regarding the use of the model response for prototype considerations. However, the model test results can be of considerable value with regard to providing an insight into the actual field response of prototype structures.

ACKNOWLEDGMENTS

The authors wish to express their appreciation to Jorj O. Osterberg, Professor of Civil Engineering, Northwestern University, for his assistance in obtaining the soil and experimental apparatus as well as his general encouragement.

The sand was provided through the courtesy of the Raymond Concrete Pile Company, Chicago.

REFERENCES

1. Kondner, R. L., "Non-Dimensional Approach to the Vibratory Cutting, Compaction and Penetration of Soils." Johns Hopkins Univ., Department of Mechanics, Tech. Report 8 (Aug. 1960).
2. Kondner, R. L., and Edwards, R. S., "The Static and Vibratory Cutting and Penetration of Soil." HRB Proc., 39:583-604 (1960).
3. Kondner, R. L., and Krizek, R. J., "A Non-Dimensional Approach to the Static and Vibratory Loading of Footings." HRB Bull. 277, 37-60 (1960).
4. Kondner, R. L., "Bearing Capacity of Friction Pile Groups in Cohesive Soil." Jour. Soil Mechanics and Foundations Division, ASCE (To be published).
5. Prakash, S., "A Review of the Behavior of Partially Embedded Poles Subjected to Lateral Loads." M.S. Thesis, University of Illinois (1960).
6. Chang, Y. C., "Annotated Bibliography of Lateral Loads on Piles." University of Illinois Report for Illinois Cooperative Highway Research Program (1960).
7. Terzaghi, K., "Evaluation of Coefficients of Subgrade Reaction." Geotechnique, Vol. 4 (Dec. 1955).
8. Czerniak, E., "Resistance to Overturning of Single, Short Piles." ASCE Proc., Vol. 83, Jour. Structural Division, Paper 1188, ST2 (March 1957).
9. Palmer, L. A., and Thompson, "The Earth Pressure and Deflection Along the Embedded Length of Pile Subjected to Lateral Thrust." Proc. 2nd Internat. Conf. on Soil Mechanics and Foundation Engineering, Vol. 5.
10. Matlock, H., and Reese, L. C., "Generalized Solutions for Laterally Loaded Piles." ASCE Proc., Vol. 86, Jour. Soil Mechanics and Foundations Division, Paper 2626, SN5 (Oct. 1960).
11. Langhaar, H. L., "Dimensional Analysis and Theory of Models." Wiley (1951).
12. Bridgman, P. W., "Dimensional Analysis." New Haven (1931).